Luminescence and electrical properties of single ZnO/MgO core/shell nanowires

Gustavo Grinblat, Francis Bern, José Barzola-Quiquia, Mónica Tirado, David Comedi, and Pablo Esquinazi

Luminescence and electrical properties of single ZnO/MgO core/shell nanowires

Gustavo Grinblat,[1] Francis Bern,[2] José Barzola-Quiquia,[2] Mónica Tirado,[3] David Comedi,[1] and Pablo Esquinazi[2,a)]

[1]*Laboratorio de Física del Sólido, Dep. de Física, FACET, Universidad Nacional de Tucumán, Tucumán, and Consejo Nacional de Investigaciones Científicas y Técnicas (CONICET), Argentina*
[2]*Division of Superconductivity and Magnetism, Institute for Experimental Physics II, University of Leipzig, D-04103 Leipzig, Germany*
[3]*Laboratorio de Nanomateriales y Propiedades Dieléctricas, Dep. de Física, FACET, Universidad Nacional de Tucumán, Tucumán, Argentina*

To neutralise the influence of the surface of ZnO nanowires for photonics and optoelectronic applications, we have covered them with insulating MgO film and individually contacted them for electrical characterisation. We show that such a metal-insulator-semiconductor-type nanodevice exhibits a high diode ideality factor of 3.4 below 1 V. MgO shell passivates ZnO surface states and provides confining barriers to electrons and holes within the ZnO core, favouring excitonic ultraviolet radiative recombination, while suppressing defect-related luminescence in the visible and improving electrical conductivity. The results indicate the potential use of ZnO/MgO nanowires as a convenient building block for nano-optoelectronic devices. © 2014 AIP Publishing LLC. [http://dx.doi.org/10.1063/1.4868648]

ZnO nanostructures have a large surface/bulk ratio, which in general is detrimental for optical applications. One of the reasons is the existence of surface defects that provide a spurious luminescence in the visible range. Moreover, adsorbed ambient molecules at the surface of the ZnO nanostructures play an important role in the relaxation processes of photo generated carriers, a sensitivity to the environment that one would like to avoid in several applications as ultraviolet (UV) photodetection. This sensitivity as well as the reset time of ZnO nanowires (NWs) can be strongly improved by surface coating with functional polymers[1] and using Schottky contacts.[1,2] An enhancement in the UV photo sensing mechanism has been achieved covering bundles of highly dense ZnO NWs with thin MgO shell[3] or depositing the NW bundles on a MgO film.[4] Whether the core-shell technique does work in single ZnO NW has not been proved yet. On the other hand, it has been recently shown that integrating a carbon nanotube and TiO_2 in a core/shell geometry with radial Schottky barriers regulates the electron transport and improves the separation of photo generated carriers increasing the photo gain while decreasing the recovery times.[5] Following this idea, in this work, we show that by covering a ZnO NW with MgO we were able to neutralise or passivate surface defects and to reduce the overall detrimental surface properties due to surface band bending. Our results demonstrate that a MgO shell, which provides confining barriers to electrons and holes within the ZnO core, enhances substantially the excitonic UV radiative recombination as well as the electrical conductivity.

Aligned ZnO NWs were grown by vapor-transport, vertically to a Au-nanoclusters-seeded amorphous SiO_2 film, following the method described in Ref. 6. The NWs on Au-seeded SiO_2 were promoted by a rough ZnO seed layer whose formation was catalysed by the Au clusters.[7] Figure 1(a) shows an example of the obtained NWs. The MgO coating of 50 nm thickness (total final diameter of the NW was 150 nm) of the ZnO NWs was also done by vapour transport deposition. Energy dispersive x-ray analysis (EDX) spectra were obtained for composition analysis across different regions along the NWs length revealing an atomic concentration ratio of (O/Mg/Zn) 48/30/19 (±2) compatible with the expected stoichiometry and the dimension of the NW. X-ray diffraction revealed the existence of both oxides with good crystalline quality and strongly preferred growth directions, i.e., for the ZnO crystal the main NW axis corresponds to (002) hexagonal wurtzite structure and for the MgO this direction corresponds to (200) of the face centered cubic structure.
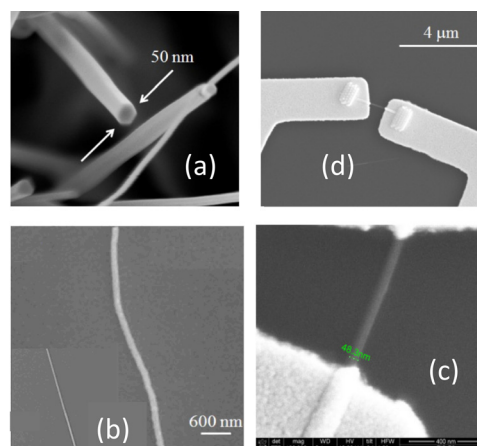

FIG. 1. Scanning electron microscope pictures of: (a) ZnO NWs before the MgO deposition. (b) Left sample is a ZnO NW and the sample in the middle of the picture is a ZnO/MgO NW. (c) One ZnO NW with its electrical contacts. The scale bar at the bottom right represents 400 nm. (d) This picture shows in less resolution a ZnO/MgO NW with its electrical contacts.

a)Electronic mail: esquin@physik.uni-leipzig.de

The core/shell NWs were then transferred to the top of a Si$_3$N$_4$/Si substrate by a printing method, i.e., a bundle of NWs is pressed between two of the aforementioned substrates. After this step, we remove big pieces and dirt by blowing air, followed by the identification of suitable NWs. We examine the samples in a Dual Beam Microscope (FEI NanoLab XT 200) and after selecting a suitable NW (see Fig. 1(b)) we fix it on the substrate using electron beam induced deposition (EBID) of WC$_x$, clearly recognised as protuberances in Fig. 1(d). This material is nearly insulating;[8] besides fixing the single NW it provides a good thermal contact of the NW to the substrate. In the following step, the substrate is covered with a resist (PMMA 950 K) for the electron beam lithography process. After developing the electrodes were sputtered with Cr/Au film of thickness of 5 and 100 nm, respectively, see Figs. 1(c) and 1(d). In the last step, the sample is contacted to a chip carrier for the transport measurements.

Current-voltage (I–V) characteristics were measured using a DC voltage Agilent 6634B power source and Keithley 182 Nanovoltmeter. Impedance spectroscopy measurements were carried out using a HP 4192A impedance analyser, in the frequency range of 10 Hz to 10 MHz at room temperature. The AC voltage amplitude was 0.5 V for all measurements. The sample was connected to the instrument by means of the HP 16047 C test fixture.

To neutralise the surface defects that give rise to spurious luminescence in the visible range the covering of the ZnO NW with a MgO shell provides a good solution since besides passivation, with its large 7.9 eV band gap, much larger than the 3.4 eV of ZnO, it forms a potential barrier confining the electrons and holes in the ZnO NW in their corresponding bands. Figure 2 shows the photoluminescence of the ZnO NW without and with the MgO shell, measured using the 325 nm line of a He-Cd laser as the excitation source. As expected the luminescence due to surface defects between 1.9 and 2.7 eV energy is strongly suppressed in the core/shell NW, where the enlarged luminescence due to the recombination of excitons occurs only in the UV. This result motivates us to pursue with the measurement of the transport behaviour of single NWs.

Figure 3 shows the I–V characteristic curve for a single bare ZnO NW as well as for a core/shell NW measured in dark and under UV illumination (400 nm light-emitting diode (LED) with 20 nm bandwidth at half maximum intensity). When traps are present at the ZnO NW walls, free charges are trapped there and the NW is charge depleted; this and the developed band bending at the surface is the origin of a very high effective resistivity. The resistance of the bare ZnO NW in dark is extremely large and beyond our instrumental resolution. Therefore, the I–V characteristic curve shown in Fig. 3 for the bare ZnO NW has been measured under ambient light (∼400 lx). When the MgO shell is deposited, traps are passivated and hence, free charges remain available to contribute to the conductivity, a phenomenon already reported for GaAs NWs.[9] The origin for the asymmetric behaviour shown in Fig. 3, for the ZnO/MgO NW, is not quite clear yet. The absence of any asymmetry in the I–V measurement of the bare ZnO NW, also measured with the two-points method, suggests that the asymmetry measured in the ZnO/MgO NW is related to the presence of the 50 nm MgO shell and, e.g., its inhomogeneous capping. The stress on the ZnO NW due to the deposition of the MgO shell on it, may have also an influence on the electrical properties of the NW, an effect that needs to be studied in detail in the future.

When the ZnO/MgO NW is illuminated with UV light the I–V curve indicates that the rectifying behaviour is suppressed due to the induced photocarriers, see Fig. 3. We realise that the nanodevice exhibits a high diode ideality factor of 3.4 below 1 V, obtained from the I–V curve in dark and at forward bias, see Fig. 3, much larger than the commonly observed factor between 1 and 2 in metal/semiconductor junctions.[10] We note that this phenomenon was observed in other metal-insulator-semiconducting nanostructures.[11] Although its origin is under discussion, one speculates that this ideality factor can be strongly influenced by the MgO insulating layer and recombination processes at interfaces due to the small dimensions of the nanostructures.

To check the intrinsic conduction mechanisms (NW bulk (core) and grain boundaries or interfaces) involved in the conducting circuit of the NW, we performed impedance spectroscopy measurements at room temperature at different
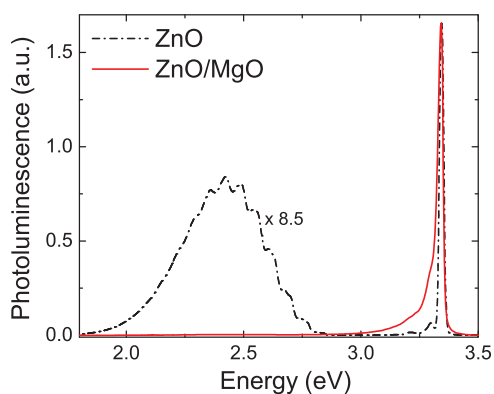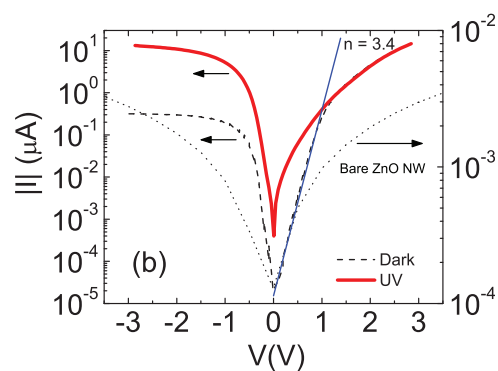

FIG. 2. Photoluminescence of the ZnO NW without (black line) and with the MgO shell (red line). Note the strong suppression of the surface defect induced luminescence and the enlargement at the UV energy range. The data for the bare ZnO NW is multiplied by a factor of 8.5 to have the same UV peak intensity as for the ZnO/MgO NW.

FIG. 3. Current-Voltage (I–V) measurements of a single bare ZnO NW at room temperature in ambient light (short dashed line), of a single ZnO/MgO in dark (dashed line) and under illumination with 400 nm light wavelength (full line) in a semilogarithmic scale. The straight line is a guide and has a slope of 3.4.

bias voltages, both, in dark and under UV. The impedance analyser was used in the averaging mode and Z/θ measurement function. Prior to the measurements, a short and open circuit calibration of the impedance analyser at all frequencies was performed, in order to account for the parasitic circuit elements connected to the sample. The calibrations were made keeping the stray impedances as close as possible to their values during the measurement: The type and position of the cables, contacts, and connectors during the calibrations were the same as during the measurement.[12]

Figure 4 shows the results of the impedance spectroscopy measurements in a Cole-Cole representation (imaginary vs. real components of the impedance) of one of the NWs at room temperature. The bias dependence in the dark is stronger than in the illuminated case, as can be expected from the I–V-curves, see Fig. 3. To understand the observed behaviour, in general, one assumes the existence of different resistances and capacitances due to the different processes that influence the conduction through the NW, taking into account not only the intrinsic conduction processes but also those from wiring and interfaces. In general, each conduction process might be modelled by a parallel resistance/capacitance (B/C) equivalent circuit with a resistance A associated with the total resistance due to external components, such as wiring, see sketch in Fig. 4. Different processes, each given by the mentioned equivalent circuit, can contribute in parallel or in series.[13] The process-related contributions can be recognised in a Cole-Cole plot by different arcs or semicircles centered at different frequencies, upon process. In the present case of our NW, see Fig. 4, a single arc is always observed. Therefore, we start with a single equivalent circuit given by the following equation:
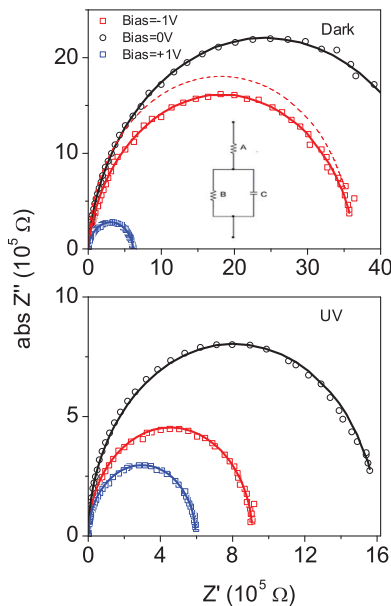
$$Z' + iZ'' = A + \left(\frac{1}{B} + i\omega C \right)^{-1}, \qquad (1)$$

where $\omega = 2\pi\nu$ denotes the used frequency and i is the imaginary number. From the fit of the data to Eq. (1), we realise that the impedance in dark cannot be fitted using a frequency independent capacitance; an example of a fit with constant C is shown in Fig. 4, by a dashed line. Leaving C as a free frequency dependent function, we extract the function $C(\nu)$ shown in Fig. 5. The achieved circuit with the NW is very near an ideal one since the capacitance decreases with frequency by only a factor of two in five orders of magnitude frequency change, see Fig. 5. The value of the resistance $A = 300 \, \Omega$ remained constant in all the measurements. The values of the resistance B obtained from the fits are (in 10^5 Ω) = 36.60, 48.50, 6.13 for -1, 0, $+1$ V bias voltage. Under UV illumination, the behaviour of the impedance is ideal, i.e., it follows the equivalent circuit depicted in Fig. 4 with all parameters frequency independent. The deduced resistance values in this case are $B(10^5\Omega) = 9.10$; 16.10; 5.95 for -1; 0; $+1$ V bias voltage. Note that under UV there is a clear decrease in the asymmetry of the resistances around zero bias voltage in comparison with the measurements in dark, in agreement with the I–V curves shown in Fig. 3. This indicates a decrease of the effective potential barrier by the induced photocarriers.

We note that the range of the obtained capacitance values ($\sim 2 \times 10^{-11}$ to $\sim 1.3 \times 10^{-10}$ F) suggests conduction mechanisms from, both, the NW bulk (core) and through interfaces to or boundaries in the MgO.[14,15] Similar measurements in the bare ZnO NW provide an equivalent, frequency independent capacitance of $C \simeq 2 \times 10^{-11}$ F. Therefore, and as an attempt to separate the NW core from an interface/boundary-related contribution, two equivalent B_i/C_i circuits (i: bulk or interface-related) were added in series achieving similar good fits to the data as those shown in Fig. 4. To fit the data in dark and under UV one needs only to change the equivalent resistances and mainly that from the bulk contribution, showing this a decrease of three orders of magnitude under UV illumination. Within this last model, the capacitance value obtained for the bulk contribution is $C \simeq 5 \times 10^{-11}$ F and $C \simeq 1 \times 10^{-10}$ F for the interface/boundary-related contribution, both, bias voltage and
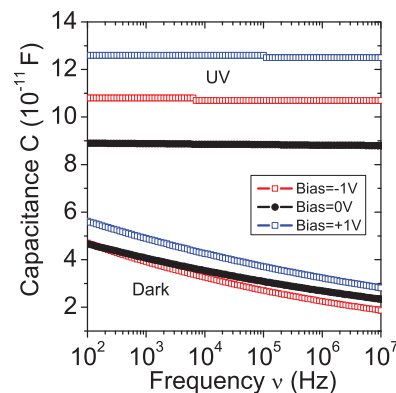
FIG. 4. Cole-Cole plot of the obtained imaginary Z'' and real Z' components of the impedance of a single ZnO/MgO NW in dark (upper figure) and under UV (lower figure) illumination at room temperature for different bias voltages. The continuous lines were obtained from the fit using the circuit depicted in the upper figure and the capacitance shown in Fig. 4 and resistance values described in the text. The dashed line was obtained using the equivalent circuit but with a frequency independent capacitance. Similar fits are obtained adding two equivalent circuits, for the bulk and for an interface/boundary-related contribution, see text.

FIG. 5. Values of the capacitance C vs. frequency obtained from the fits to the experimental results shown in Fig. 4 in dark (lower curves) and under UV (upper curves) within the simple equivalent circuit shown in Fig. 4(a).

frequency independent, in dark and under UV illumination. This result indicates that both parts contribute in the conduction mechanism of the ZnO/MgO NW.

In conclusion, we have prepared and isolated ZnO/MgO core/shell NWs and contacted them using a combination between electron beam induced deposition and electron beam lithography for electronic transport measurements. The photoluminescence and electrical characterisation indicates an effective passivation of the ZnO surface through MgO. Impedance spectroscopy measurements indicate that in the nano circuit, a bulk as well as an interface/boundary-related contribution takes part in the conduction process.

[1] J. Zhou, Y. Gu, Y. Hu, W. Mai, P.-H. Yeh, G. Bao, A. K. Sood, D. L. Polla, and Z. L. Wang, Appl. Phys. Lett. **94**, 191103 (2009).

[2] M. W. Chen, C. Y. Chen, D. H. Lien, Y. Ding, and J. H. He, Opt. Express **18**, 14836 (2010).

[3] Y. Wu, W. Wu, X. M. Zou, L. Xu, and J. C. Li, Mater. Lett. **84**, 147 (2012).

[4] D. C. Kim, B. O. Jung, J. H. Lee, H. K. Cho, J. Y. Lee, and J. H. Lee, Nanotechnology **22**, 265506 (2011).

[5] C.-Y. Hsu, D.-H. Lien, S.-Y. Lu, C.-Y. Chen, C.-F. Kang, Y.-L. Chueh, W.-K. Hsu, and J.-H. He, ACS Nano **6**, 6687 (2012).

[6] G. Grinblat, M. G. Capeluto, M. Tirado, A. V. Bragas, and D. Comedi, Appl. Phys. Lett. **100**, 233116 (2012).

[7] N. C. Vega, R. Wallar, J. Caram, G. Grinblat, M. Tirado, R. R. LaPierre, and D. Comedi, Nanotechnology **23**, 275602 (2012).

[8] D. Spoddig, K. Schindler, P. Rödiger, J. Barzola-Quiquia, K. Fritsch, H. Mulders, and P. Esquinazi, Nanotechnology **18**, 495202 (2007).

[9] A. C. E. Chia, M. Tirado, F. Thouin, R. Leonelli, D. Comedi, and R. R. LaPierre, Semicond. Sci. Technol. **28**, 105026 (2013).

[10] S. M. Sze, *Physics of Semiconductor Devices* (John Wiley & Sons Ltd., New York, 1982).

[11] M. Özer, D. E. Shildiz, S. Altindal, and M. M. Bülbül, Solid-State Electron. **51**, 941 (2007).

[12] C. Grosse and M. Tirado, IEEE Trans. Instrum. Meas. **50**, 1329 (2001).

[13] S. M. Haile, D. L. West, and J. Campbell, J. Mater. Res. **13**, 1576 (1998).

[14] *Impedance Spectroscopy: Theory, Experiment, and Applications*, edited by E. Barsoukov and J. R. MacDonald (John Wiley & Sons, Inc., New York, 2005).

[15] J. T. S. Irvine, D. C. Sinclair, and A. R. West, Adv. Mater. **2**, 132 (1990).